Energetics of the Florida Current

by Irving H. Brooks[1] and Pearn P. Niiler[2]

ABSTRACT

During the summer of 1974, fifty free-drop transport profiles and STD/XBT profiles were carried out in the Florida Current at 14 stations along the 25°51.00′ N latitude. From these data and from the historical free-drop data 12 km to the south, a computation is made of the energy flow from the mean current to the fluctuations over the entire cross-section of the Florida Straits. Statistically significant areas of both potential and kinetic energy conversion are computed. In the absence of the influence of pressure gradients on the energy flux, a local transfer can occur both to and from the fluctuations. The net flux over the cross-sectional area is not significant; it would lead to a decay time of total perturbation energy in 50 days which is far in excess of the time required for the water mass of the Florida Current to travel through the Straits of Florida. We conclude that pressure forces must locally balance the energy flow so that an equilibrium exists between the fluctuations and the mean Florida Current.

1. Introduction

Along the eastern seaboard of North America, from the Florida Keys to Cape Hatteras, North Carolina, the Florida Current is a strong and persistent flow from the ocean surface to the bottom (Richardson, Schmitz and Niiler, 1969). Significant nontidal, temporal variability of this flow is documented (Niiler and Richardson, 1973; Düing, 1975; Niiler, 1975; Webster, 1961b), and calculations show that a transfer of energy between the mean current and the fluctuations can exist on the ocean surface (Webster, 1961a, 1965; Oort, 1964; Schmitz and Niiler, 1969). Reliable estimates of the rate of energy transfer, however, have not been available until now because of the lack of simultaneous time-series of the density, velocity, and sea-level variations within the current. During the period May 16 through August 13, 1974, we made fifty excursions into the Florida Straits at 25°51.00′N to obtain a set of simultaneous measurements of horizontal currents, temperature, and salinity from the ocean surface to the bottom at fourteen stations by the free-drop method (Richardson and Schmitz, 1965; Richardson, Carr and White, 1969). A near-bottom array of current meters and bottom pressure gauges was also main-

1. Physical Oceanography Laboratory, Nova University, Dania, Florida, 33004, U.S.A.
2. School of Oceanography, Oregon State University, Corvallis, Oregon, 97331, U.S.A.

tained in the Straits of Florida during this period. The primary purpose for this array was to test the adequacy of the statistics derived from the free drop measurement scheme. It has been learned that other useful information could be gained from the array data. Analyses of these time series are presented in this issue of JMR by Wunsch and Wimbush (1977), Düing, Mooers and Lee (1977), and Lee and Mayer (1977). Here we present the calculations of the vertical and horizontal distributions of the energy exchange between the fluctuations and the mean flow obtained from the free-drop data set. Analysis of the variability of the transport through the Straits of Florida obtained by the free-drop method during this period is presented by Brooks (1977).

The estimate of the energy flux from the mean flow to the fluctuation primarily depends upon how the mean flow is defined. Three-month time series of temperature, velocity, and electric potential across submarine cables in any particular season at various locations in the Straits of Florida reveal that the greater portion of the variance is accounted for by fluctuations with periods less than 20 days (and greater than 12 hours). Significant seasonal differences in the flow regime, however, are also reported (Niiler and Richardson, 1973). There appears to be a spectral gap between the yearly period and the 14 to 12 day period fluctuations. Therefore, it is feasible to calculate interactions between a seasonal mean flow and the variability during that season because the influence of a large number (greater than ten) of energetic events occurs during a season, which can be measured within a field program of reasonable length and scope. The contribution to the energy exchange rate from the seasonal period variations is not estimated in this calculation; we know, however, that such a contribution can be as large as the rate of exchange we present here. This conclusion is based on the observation that the seasonal differences in the mean-flow parameters within the Straits are as large as the variability seen on the aforementioned shorter time scales (Niiler and Richardson, 1973).

We chose to use the free-drop system for this observational program because it appeared to be the most cost effective system for the study of variability in a mean flow in excess of 50 cm/sec. However, sacrifices of vertical and temporal resolution in the measurements, particularly in the horizontal current field, had to be made. Within the Straits a vertically averaged current over a depth interval of 100 m can be measured with a dropsonde to an accuracy of 1 to 2 cm/sec (instrument displacements of 1 to 2 m, Schmitz, 1966). It is possible to make five measurements at each location within a week. Energy exchange can also occur on vertical scales which are smaller than those over which we averaged, or on shorter time scales which we did not adequately resolve. Near the bottom, the velocity field can exhibit an especially strong vertical shear (20 cm/sec over a 20 m interval; Weatherly, 1972). The energy exchange can be modified by boundary layer processes which are not resolved in the free-drop data set. When we began this experiment, we

believed that the bottom layer was confined, at most, to a 20 m column above the bottom, and that a fixed level array at 50 m above the bottom would yield useful data by which the adequacy of our temporal sampling scheme could be verified across the entire Straits. However, during the course of the experiment, it became evident through STD and XBT profiles that homogeneous columns of water (the bottom boundary layers) extend 50 to 100 m above the bottom (Weatherly and Niiler, 1974). At only three locations were current meters emplaced more than 50 meters above the bottom. There, the energy levels of the free drop data and the fixed level sensors are within the standard errors.

For any field variable or derived quantity, $\phi\ (t_n, \vec{x}_j)$, which has been measured n times at j locations, the sample mean value is defined as $\bar{\phi}\ (\vec{x}_j) = \{\sum_n \phi\ (t_n, \vec{x}_j)/n\}$. The standard error of the mean is computed from the expression $\epsilon = \{\sum_n (\bar{\phi} - \phi)^2/n(n-1)\}^{\frac{1}{2}}$. The variability in the Straits is known to be energetic with periods greater than the semidiurnal. At any one station, our data were taken at least sixteen hours apart. Although we assume that these free-drop measurements are statistically independent, we are fully aware that energetic peaks in the variability appear at periods of 12 to 14 days (Wunsch and Wimbush, 1977). If we were to consider data to be statistically independent only if measurements were made at least forty hours apart, the standard errors at the mean would be increased by approximately twenty-five percent. Our treatment of the data is identical to that in existing publications on the energetics of the Florida Current.

There were 41 cruises completely across the Straits in the summer of 1974 at 25°51.00′N. The mean northward transport within the Florida Straits during this time was $33.3 \pm 0.4 \times 10^6 m^3/sec$. The free-drop measurements taken at the Virginia Key latitude of 25°44.5′N (12.0 km to the south) during the summers of 1965, 1968, and 1969) account for 12 complete cruises, with a mean transport of $33.5 \pm 0.9 \times 10^6 m^3/sec$. The $\pm$ quantity is the standard error of the mean. Over this spatial interval, there are significant downstream adjustments of the mean Florida Current structure (Schmitz, 1969). Because the total northward transport of both sections are the same, the historical data is used for estimating the downstream changes of the mean distributions between the 1974 section and the Virginia Key section. These estimates are needed for the computation of the energy exchange. This presentation does not exhaust the dynamical information which is contained in these unique data sets; all the data used here is available on accessible Fortran format at Nova University.

2. The energy balance of the fluctuating field

Let the velocity field be expressed as $\vec{v}(\vec{x}, t_k) = \bar{\vec{v}}(\vec{x}) + \vec{v}'(\vec{x}, t_k)$ as a function of position $\vec{x}$ and time t_k, and let $\rho = \bar{\rho} + \rho'$ and $p = \bar{p} + p'$ be similar decomposition

density and pressure fields. The overbar denotes the average over the measurements taken at times t_k, and the prime denotes the fluctuation quantity. The approximate equations which govern the evolution of the mean intensity of the fluctuations are

$$\frac{d}{dt}\{\tfrac{1}{2}(\overline{u'^2}+\overline{v'^2})\} = -\nabla\cdot\frac{\overrightarrow{v'p'}}{\rho_o} - g\frac{\overline{w'\rho'}}{\rho_o}$$

$$-\overline{u'^2}\frac{\partial\bar{u}}{\partial x} - \overline{v'^2}\frac{\partial\bar{v}}{\partial y} - \overline{u'v'}\frac{\partial\bar{v}}{\partial x} - \overline{w'v'}\frac{\partial\bar{v}}{\partial z} - \overline{w'u'}\frac{\partial\bar{u}}{\partial z}\,, \tag{1}$$

$$\frac{d}{dt}\{\tfrac{1}{2}\overline{\rho'^2}\} + \overline{u'\rho'}\frac{\partial\bar{\rho}}{\partial x} + \overline{v'\rho'}\frac{\partial\bar{\rho}}{\partial y} + \overline{w'\rho'}\frac{\partial\bar{\rho}}{\partial z} = 0 \tag{2}$$

where u, v, w are positive eastward, northward and upward respectively. In the above momentum equations, we use the Boussinesq approximation and the hydrostatic balance; it is assumed that $\partial\bar{v}/\partial x >> \partial\bar{u}/\partial y$. The contributions to the advection of energy by the fluctuating components and kinetic energy and density dissipations are omitted; $\frac{d}{dt}$ is the rate of change following the mean flow (these equations are derived in a variety of references—for example, see Lumley and Panofsky, 1964). In specific hydrodynamic situations, the terms on the right-hand side of (1) can be identified as primary sources of energy exchange between the mean flow and fluctuations. For example, in relatively simple conditions where $\bar{u} = 0$, $\bar{v} = \bar{v}(x,z)$, $\bar{w} = 0$, and $\bar{\rho} = \bar{\rho}(x,z)$ there can be a release of mean potential energy to the fluctuations through growing, small-amplitude waves through the term $g\overline{w'\rho'}/\rho_o$ (the "baroclinic" instability). There can also be a release of mean kinetic energy through the term $\overline{w'v'}\frac{\partial\bar{v}}{\partial z}$ (the Kelvin-Helmholtz instability) or $\overline{u'v'}\frac{\partial\bar{v}}{\partial x}$ (the "barotropic" instability). Which process dominates in small amplitude wave interactions depends upon the horizontal and vertical scales of $\bar{v}$ and $\bar{\rho}$. Of course, not even the simplest theory of fluctuation interactions with the mean flow in a three-dimensional mean flow pattern in the Florida Straits has been developed. If some single term on the right-hand side of Equation (1) dominates the energy exchange process—even in this complex situation—there would be a strong indication that one specific physical process is in operation, and a great deal of insight could be gained from simple models which are mentioned above. But as we shall subsequently see, this is not the case.

Equations (1) and (2) can be combined into a single, total energy equation by eliminating $\overline{w'\rho'}$,[3]

3. It can be shown from measurements that

$$\tfrac{1}{2}\overline{\rho'^2}\frac{d}{dt}\{1 \Big/ \left|\frac{\partial\bar{\rho}}{\partial z}\right|\} << \overline{u'\rho'}\frac{\partial\bar{\rho}}{\partial x} \Big/ \left|\frac{\partial\bar{\rho}}{\partial z}\right| \quad .$$

Table 1. Net Energy Exchange Rate in the Florida Straits. Negative quantities represent a transfer of energy to fluctuations; brackets { } indicate integral values over cross-sectional area of 3.73×10^{11} cm^2.*

Quantity	Units	Net value	Net absolute value	Net standard error
$\bar{\rho}\left\{\overline{u'v'}\frac{\partial \bar{v}}{\partial x}\right\}$	ergs cm^{-1}sec^{-1}	-32×10^6	572×10^6	551×10^6
$\bar{\rho}\left\{\overline{u'^2}\frac{\partial \bar{u}}{\partial x}\right\}$	ergs cm^{-1}sec^{-1}	89×10^6	135×10^6	143×10^6
$\bar{\rho}\left\{\overline{v'^2}\frac{\partial \bar{v}}{\partial y}\right\}$	ergs cm^{-1}sec^{-1}	3×10^6	2048×10^6	484×10^6
Sum of terms in Line 3c	ergs cm^{-1}sec^{-1}	60×10^6	2124×10^6	1178×10^6
$\left\{g\overline{u'\rho'}\frac{\partial \bar{\rho}}{\partial x} \Big/ \left\lvert\frac{\partial \bar{\rho}}{\partial z}\right\rvert\right\}$	ergs cm^{-1}sec^{-1}	-233×10^6	376×10^6	471×10^6
$\left\{g\overline{v'\rho'}\frac{\partial \bar{\rho}}{\partial y} \Big/ \left\lvert\frac{\partial \bar{\rho}}{\partial z}\right\rvert\right\}$	ergs cm^{-1}sec^{-1}	228×10^6	985×10^6	643×10^6
Sum of terms in Line 3d	ergs cm^{-1}sec^{-1}	-5×10^6	1067×10^6	1115×10^6
Total energy flux, sum of terms in Lines 3c, 3d	ergs cm^{-1}sec^{-1}	55×10^6	2394×10^6	2292×10^6
$\bar{\rho}\left\{\frac{\overline{u'^2}}{2} + \frac{\overline{v'^2}}{2}\right\}$	ergs cm^{-1}	135×10^{12}		31×10^{12}
$\left\{g\frac{\overline{\rho'^2}}{2} \Big/ \left\lvert\frac{\partial \bar{\rho}}{\partial z}\right\rvert\right\}$	ergs cm^{-1}	102×10^{12}		26×10^{12}
Total fluctuation energy density, Line 3a	ergs cm^{-1}	237×10^{12}		57×10^{12}

* The integration is carried out over an area bounded by the following depths and stations:

Station	3	4	5	6	7	8	9	10	11	12
Depth (m)	125	275	275	275	300	600	725	750	750	575

$$\frac{d}{dt}\{\tfrac{1}{2}(\overline{u'^2} + \overline{v'^2}) + \frac{g}{2}\overline{\rho'^2} \Big/ \left\lvert\frac{\partial \bar{\rho}}{\partial z}\right\rvert \rho_o\} = \tag{3a}$$

$$-\nabla \cdot \{\overrightarrow{\overline{v'p'}}/\rho_o\} \tag{3b}$$

$$-\{\overline{u'^2}\frac{\partial \bar{u}}{\partial x} + \overline{v'^2}\frac{\partial \bar{v}}{\partial y} + \overline{u'v'}\frac{\partial \bar{v}}{\partial x}\} \tag{3c}$$

$$-\{g\overline{u'\rho'}\frac{\partial \bar{\rho}}{\partial x} \Big/ \rho_o \left\lvert\frac{\partial \bar{\rho}}{\partial z}\right\rvert + g\overline{v'\rho'}\frac{\partial \bar{\rho}}{\partial y} \Big/ \rho_o \left\lvert\frac{\partial \bar{\rho}}{\partial z}\right\rvert\} \tag{3d}$$

$$-\{\overline{w'u'}\frac{\partial \bar{u}}{\partial z} + \overline{w'v'}\frac{\partial \bar{v}}{\partial z}\} \quad . \tag{3e}$$

From our 1974 free-drop data set and data gathered in the summers of 1965, 1968, and 1969, we compute statistically significant distributions of each term in the total fluctuation energy distribution in line (3a), the exchange flux of kinetic energy in line (3c) and the potential energy exchange rate in line (3d).

The following sections present, in more detail, the method of handling the data and the individual distributions of the variables which went into the calculations. The principal conclusions of our calculations are presented on Table 1. The following is a summary of these conclusions.

a) Qualitatively, the surface distribution of $\overline{u'v'}\ \partial\bar{v}/\partial x$ is the same as was previously reported by Schmitz and Niiler (1969). Our calculation yields a smaller magnitude of this function. This difference is anticipated because the data sets used in earlier investigations also include measurements from the winter season in the averages. The vertical and horizontal distribution of $\overline{u'v'}$ at 25°51.00'N (1974 data) compares favorably with the summer distribution computed at the Virginia Key latitude section (1965, 1967, and 1969 combined). The surface distribution of $\overline{u'T'}$ is qualitatively similar to that calculated by Oort (1964) off Jacksonville, Onslow Bay, and Cape Hatteras.

b) There is significant horizontal and vertical depth dependence in all of the distributions. Typically, a node exists in the horizontal or vertical in the terms on the right-hand side of equation (3); both positive and negative values occur in all the distributions. Locally, no single term dominates the energy exchange. On the left-hand side of equation (3), there appears to be an equipartition of energy between potential and kinetic energy.

c) The averages over the area of terms in line (3c) are significantly smaller than their mean absolute values. The area average of the first term in line (3d) nearly cancels that of the second term. There is no significant exchange of energy between the mean flow and the fluctuations over the sectional area. Following the mean motion, the time scale for decay of the energy of the perturbations is 2 months. Because over the cross-sectional area, the flux of energy to the fluctuations is of opposite sign and equal to the flux of the mean flow, and because the kinetic energy density of the mean flow is much larger than that of the fluctuations, the doubling time for the energy of the mean flow is much larger.

d) Local, total energy conversion is significant. In the absence of work done by pressure forces, the local doubling times for the fluctuation energy are a few days. This rapid exchange is not consistent with the area average picture in which the pressure forces can do little work (the area average of $\nabla \cdot \overrightarrow{v'p'}$ nearly vanishes). We conclude that the local energy balance cannot be determined without considering, in detail, the pressure field. This is hardly a startling conclusion; however, it needs to be stated emphatically for this flow regime.

Our conclusions bear out the suggestion by Schmitz and Niiler (1969) that sig-

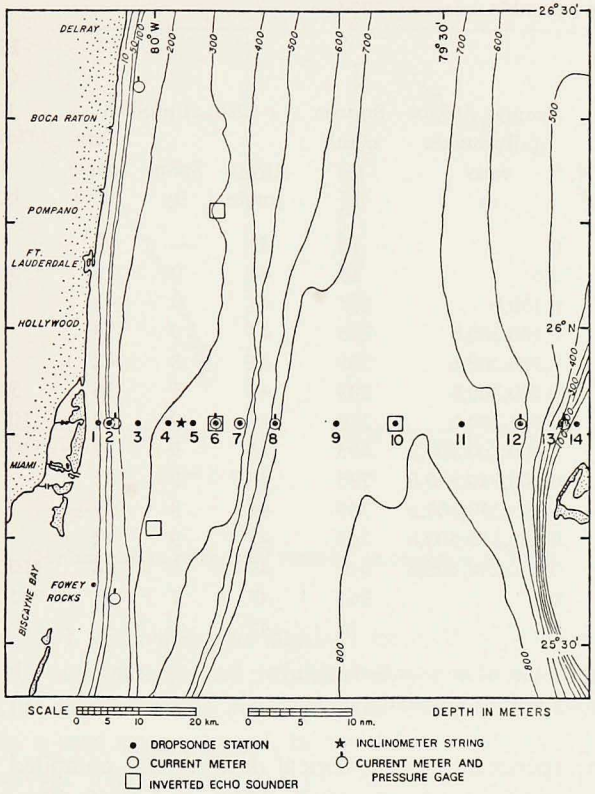

Figure 1. Schematic of the topography of the Florida Straits and location of the experiment in the summer of 1974.

nificant local energy conversions can appear within the water mass, but only an internal adjustment is occurring with no net conversion.

3. The experiment

Fig. 1 displays the location of the experiment in the Straits of Florida. Table 2 presents a summary of the free-drop data set which we compiled in the summer of 1974. During each cruise, the mid-depth instruments traveled to a somewhat different depth than that shown in Table 2. The actual depth was determined from the time the instrument travels under water. We calibrated each release-dropsonde-weight combination before the experiment for both rise rates and fall rates; with this information we estimate that we can ascertain the actual depth to which a dropsonde travels to within 2%. We anticipated using a freely-dropped STD (Bissett-Berman model 9060) as the bottom dropsonde; however, the STD electronics failed after 23 cruises, so the temperature field was measured by XBT's for the

Table 2. Free-drop ensemble, summer, 1974.

Station No.	Distance east of 25°51.00'N 80°6.98'W	Average depths of dropsonde casts m	Bottom depth (b) m	No. of profiles			Fixed level sensors	
				Dropsonde	Salinity	Temperature	Current meters (distance above bottom)	Bottom pressure record
1	2.0	0	10	43	—	—		
2	4.1	0,b	85	44	9	15	* 50m, 10m	x
3	9.0	0,100,b	245	44	9	41		
4	13.9	0,100,200,b	275	45	9	39		
5	18.1	0,100,200,b	305	45	8	42		
6	22.3	0,100,200,b	285	45	7	36	50m, 10m	x
7	26.5	0,100,200,b	310	45	9	40	100m	
8	32.6	0,100,200,400,b	605	45	9	37	*100m, 10m	x
9	43.3	0,100,350,500,b	735	45	9	41		
10	53.9	0,100,350,500,b	785	46	8	37		
11	64.6	0,100,350,500,b	765	47	9	42		
12	75.3	0,100,200,400,b	610	47	8	36	†100m	x
13	82.1	0,b	365	47	7	41	* 50m	
14	84.7	0	10	45	—	—		

* Mooring is slightly east of dropsonde station.

† Mooring is slightly west of dropsonde station.

remainder of the experiment. The historical data set was compiled in various periods between May and September in 1965, 1968, and 1969. The specific dates of the cruises and the station locations of this data set are tabulated by Niiler and Richardson (1973). In the historical data base, there are typically 6 STD profiles and 20 dropsonde profiles per station. The vertical sampling scheme of the dropsondes in the historical data varies somewhat from cruise to cruise; however, it was consistent with the one used in 1974.

The vertical distribution of the horizontal velocity field is computed from each set of dropsonde observations by least square fitting of a cubic spline function to the measured "instantaneous" values of the vertically averaged current as a function of depth. The spline fit to the vertically averaged velocity to depth z is given by $\vec{v}_s(z) = \sum_{k=0}^{3} \vec{a}_k z^k$. The velocity is derived from an analytic differentiation of the expression $\vec{v}(z) = \frac{\partial}{\partial z}\{z\vec{v}_s(z)\}$. The values of $\vec{v}$ every 25 m from the surface to the bottom are compiled and all quantities are computed at these levels. Contours of the computed quantities are constructed by determining the locations of isopleths by linear interpolations both between the 25 m interval points and between the stations. The contouring procedures contained implicit errors of ±12.5 meters in the vertical and ±0.5 kilometers in the horizontal.

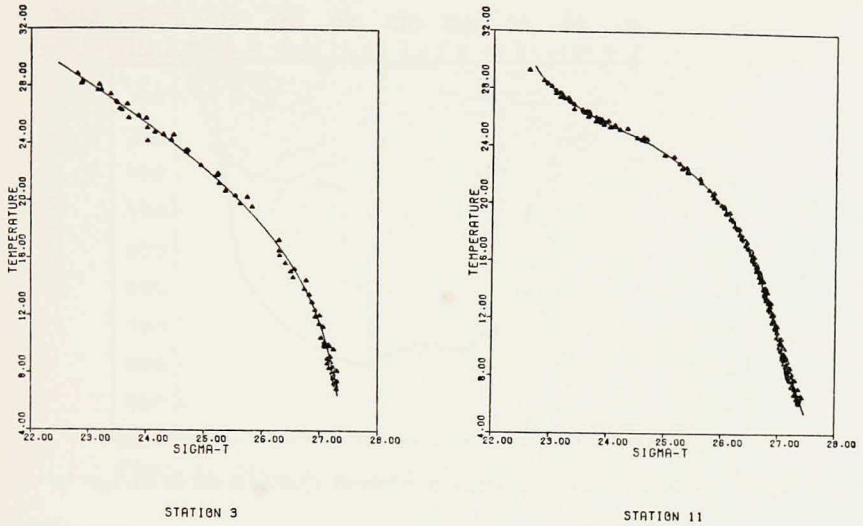

Figure 2. The temperature-density correlation function at Stations 3 and 11.

The STD and XBT data was also digitized on a 25 m interval. The density is computed from the temperature and salinity data gathered when the STD was operational. The STD data is used to define a density-temperature correlation function at each station by a least square quartic fit through the data over selected temperature and σ_t intervals. Fig. 2 displays a plot of the density-temperature data for Stations 3 and 11 as well as the least square quartic function. We see that the water mass in the western side of the Straits is not as stationary as it is in the eastern side, presumably because at times the Florida Shelf water and the Gulf of Mexico surface water influence the water mass (Iselin, 1937). We estimate that an inaccuracy of 0.15 in σ_t is made in the western side of the Straits by using the water mass correlation method; the natural root mean square variation of σ_t in this area is 0.60.

In our presentation of the uncertainties (or errors) of the average values of dynamical quantities, the random errors of measurements are not included. Summarizing the previous error analysis of the dropsonde-STD-XBT system and adding our own conservative experimental error estimates, we find that the average velocity over 100 ± 2 m depth interval is measured to within 2 cm/sec; temperature is measured to an accuracy of ±0.2°C, salinity to an accuracy of ±0.05‰ and σ_t to ±0.1. Because these errors are random and the data base is relatively large, their influence on determining the accuracy of the means is smaller than the standard error of a mean induced by the natural intense variability.

4. The mean field

Fig. 3 displays the distributions of the mean dynamical variables from the 1974

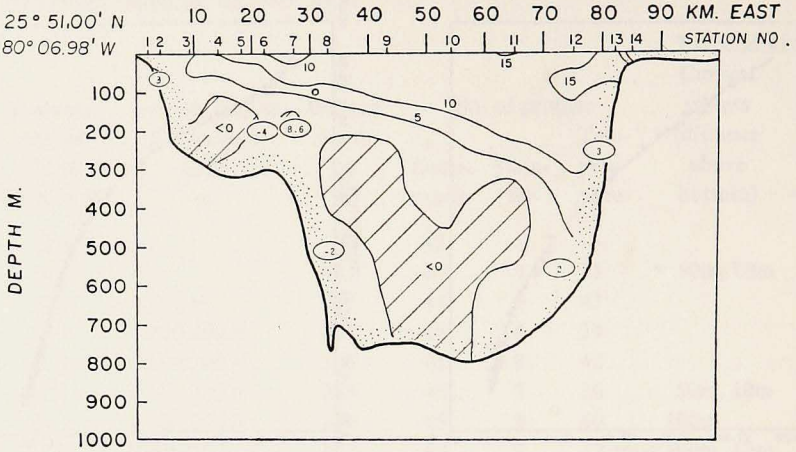

Figure 3a. Mean eastward velocity component. Contours are in cm sec^{-1}.

free-drop data set. Selected contours of $\bar{v}$ and $\overline{\sigma_t}$ from the historical data are superimposed on these graphs. The area near the bottom is speckled on these figures; as discussed earlier, there are serious limitations in interpreting free-drop velocity data in this region. A mean derived from the current meter data is superimposed on the horizontal velocity and temperature distributions. This mean is circled and is located at the sensor location.

Together with the mean values, we also compute the standard errors of these means at each level. Table 3 presents a list of the maximum and minimum standard errors of the mean which were incurred between Stations 3 and 12. This is the area

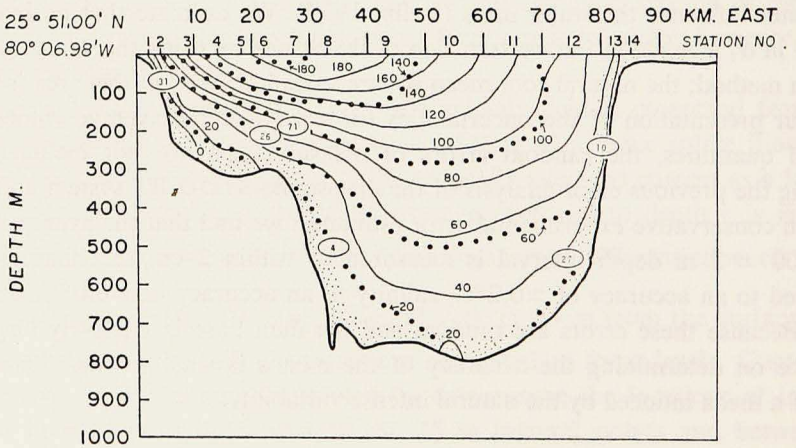

Figure 3b. Mean northward velocity component. Contours are in cm sec^{-1}. Dotted curves are from historical summer data, 12 km to the south.

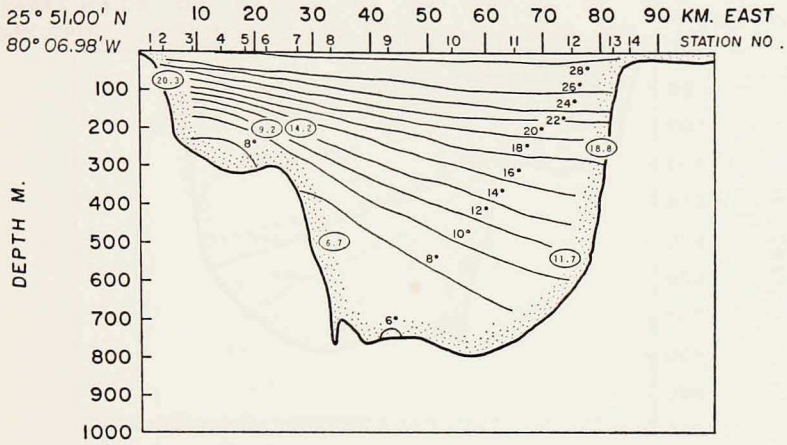

Figure 3c. Mean temperature distribution. Contours are in °C.

Table 3. Maximum and minimum standard errors of the mean fields between Stations 3 and 12.

Variable	Maximum std. error	Station No; Depth, m.	Minimum std. error	Station No; Depth, m.
$\bar{u}$(cm/sec)	3	5;75	1	11;300
$\bar{v}$(cm/sec)	9	3;0	2	9,10,11;500
$\bar{T}$(°C)	0.5	3;100	0.1	10;775
$\bar{S}$(‰)	0.1	6,7,8;175	<0.01	8,9,10;bottom
$\overline{\sigma_t}$	0.11	3;75	0.01	8,9,10;bottom

in which meaningful energy flux calculations can be made because of the overlay between the 1974 data and historical data. It should be noted that some of the current meter values differ from the respective dropsonde values by slightly more than

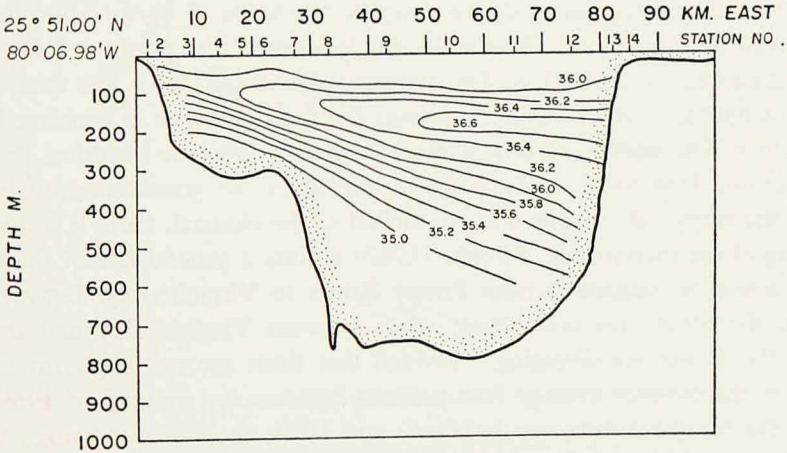

Figure 3d. Mean salinity distribution. Contours are in ‰.

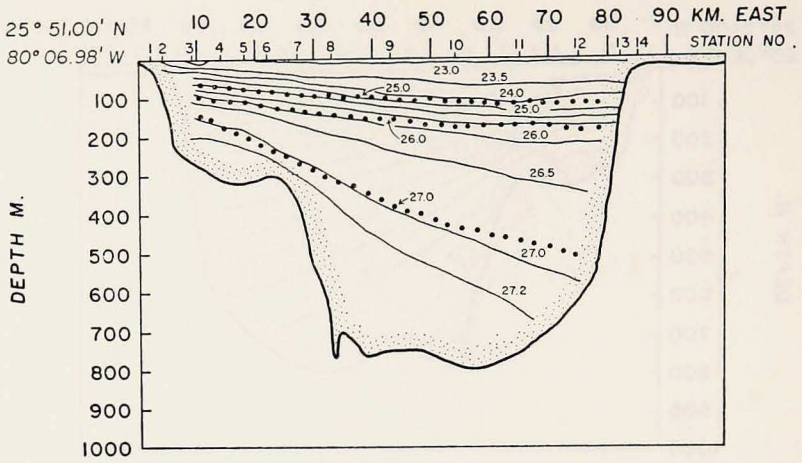

Figure 3e. Mean density distribution. Contours are in σ_t units. Dotted curves are from historical summer data, 12 km to the south.

the maximum standard error which is computed solely from dropsonde data. We can ascertain no particular pattern in these deviations.

No surprising new features are found in these mean distributions. There is a strong eastward flow on the eastern side of the Straits where the coastline diverges into the Northwest Providence Channel. A general westward drift is found below the main thermocline, and an eastward flow above the thermocline is in agreement with the cross-channel flow reported by Schmitz (1969) and Niiler and Richardson (1973). Schmitz (1969) also describes an adjustment in the density and northward velocity fields between two sections which were occupied in a similar experiment at the latitude of Fowey Rocks and Virginia Key in the summer of 1965. As reported by Schmitz, the surface expression of the Florida Current axis (location of the maximum value of $\bar{v}$) shifts eastward. We compute the value of $\partial\bar{v}/\partial y$ from the $\bar{v}$ distributions in these sections. There is an acceleration of the northward flow above 200 m and a deceleration below. The average value of $(\partial\bar{v}/\partial y)$ is less than 10% of its mean amplitude, which simply expresses the fact that mass is conserved within the data sets. The northward flow is more baroclinic than the historical data from further south. This baroclinicity is also reflected in the geostrophically balanced slope of the isopycnals. In the eastern portion of the channel, there is a northward deepening of the thermocline. Schmitz (1969) reports a general rise of the thermocline of a similar magnitude from Fowey Rocks to Virginia Key. Between these latitudes, the Straits are converging, while between Virginia Key and the 1974 Section, the Straits are diverging. Provided that there are no long-term temporal changes in the summer average flow patterns between the summer of 1969 (when most of the historical data was gathered) and 1974, the density changes between the sections are interpreted as spatial—they certainly are statistically significant.

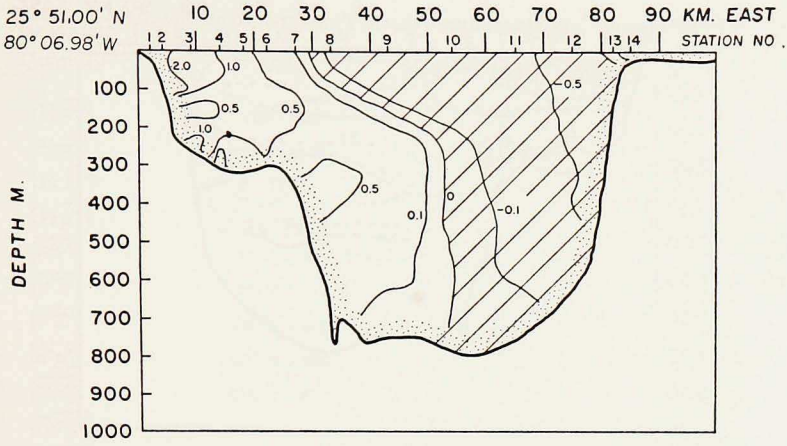

Figure 4. The Rossby number distribution, $R_o = \frac{1}{f}\frac{\partial \bar{v}}{\partial x}$.

A number of derived quantities are of dynamical interest for the modeling of variability and energy transfer processes in the Florida Current. Some of these are computed from the $\bar{v}$ and $\overline{\sigma_t}$ distributions in Fig. 3. Fig. 4 displays the Rossby number, Fig. 5 displays the Richardson number, and Fig. 6 displays the potential vorticity distribution. Again, selected contours from the historical summer data are superimposed on these figures. As defined, the Rossby number is a measure of the ageostrophic downstream momentum balance in the Florida Current, and it is clear that the mean Florida Current is not entirely in geostrophic balance. The Richardson number is a measure of the vertical stability of the mean flow. In a broad region of

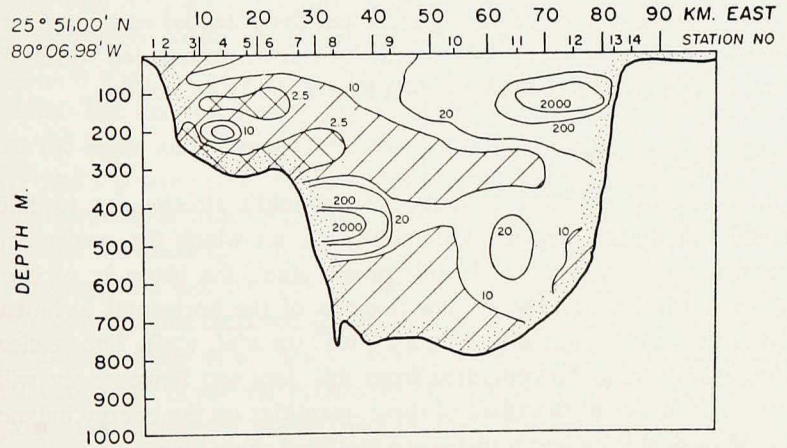

Figure 5. The Richardson number distribution, $R_i = \frac{g}{\rho_o}\left|\frac{\partial \bar{\rho}}{\partial z}\right| \Big/ \left(\frac{\partial \bar{v}}{\partial z}\right)^2$.

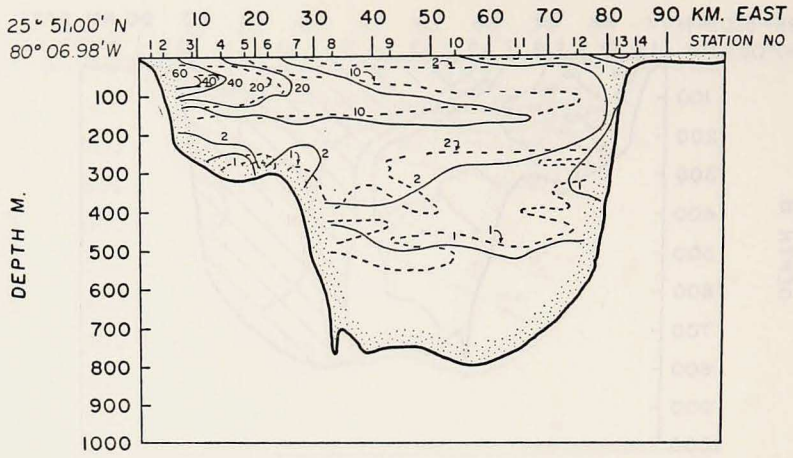

Figure 6. The potential vorticity distribution, $P = \frac{1}{\rho_o}\left|\frac{\partial \bar{\rho}}{\partial z}\right|\left(\frac{\partial \bar{v}}{\partial x} + f\right) + \frac{1}{\rho_o}\frac{\partial \bar{\rho}}{\partial x}\frac{\partial \bar{v}}{\partial z}$. The dotted areas are from historical summer data, 12 km to the south. The contours are in units of 10^{-12}cm^{-1}sec^{-1}.

the Current, the Richardson number is of order ten, and on the continental rise, the Richardson number is of order unity. Both the historical data and the 1974 data show similar distributions. The regions of low Richardson number could be regions of strong, local, vertical mixing. We know of no other evidence that vertical mixing actually does take place. The spectra of existing current meter records do not show an unambiguous dependence of internal wave energy on the Richardson number. The potential vorticity distribution shows a relatively monotonic decrease in the horizontal, but a distinct maximum appears at mid-depth where the potential vorticity gradient vanishes. This data suggests that a three layer model of the Florida Current would be needed to adequately represent the potential vorticity distribution. No systematic changes in the potential vorticity can be ascertained within the short spatial interval from the latitude of Virginia Key to the 1974 section.

5. The Reynold's stresses

In a three-dimensional flow pattern, the Reynold's stresses, or turbulent momentum and heat fluxes, depend upon the plane on which the projection of the stress vector (or tensor) is made. In this presentation, the plane is, of course, the east-west section in Fig. 1. The six components of the horizontal turbulent fluxes of interest are $\overline{u'^2}$, $\overline{v'^2}$, $\overline{T'^2}$ (or $\overline{\rho'^2}$), $\overline{u'v'}$, $\overline{u'T'}$, $\overline{v'T'}$ (or $\overline{u'\rho'}$, $\overline{v'\rho'}$). The vertical fluxes ($\overline{w'u'}$, $\overline{w'v'}$, $\overline{w'T'}$) cannot be computed from this data set; however we will subsequently make estimates of the effect of these quantities on the energy balance based on models of vertical turbulent transfer in a stratified shear flow.

The standard error of the mean of each of the above quantities is a useful, al-

Table 4. Mean absolute values of Reynold's Stress components and correlation coefficients.

Quantity	Units	Mean Absolute Value	Mean Error
$\lvert\frac{1}{2}\overline{u'^2}\rvert$	cm^2/sec^2	77	16
$\lvert\frac{1}{2}\overline{v'^2}\rvert$	cm^2/sec^2	286	66
$\lvert\frac{1}{2}\overline{T'^2}\rvert$	$°C^2$	0.68	0.17
$\lvert\frac{1}{2}\overline{\rho'^2}\rvert$	σ_t units	0.028	0.006
$\lvert\overline{u'v'}\rvert$	cm^2/sec^2	69	45
$\lvert\overline{u'T'}\rvert$	cm°C/sec	2.0	2.1
$\lvert\overline{v'T'}\rvert$	cm°C/sec	7.9	4.3
$\lvert\overline{u'\rho'}\rvert$	cm-σ_t/sec	0.35	0.40
$\lvert\overline{v'\rho'}\rvert$	cm-σ_t/sec	1.35	0.72
$\lvert R\overline{u'v'}\rvert$	—	0.27	—
$\lvert R\overline{u'\rho'}\rvert$	—	0.16	—
$\lvert R\overline{v'\rho'}\rvert$	—	0.31	—

though not the exclusive, measure of the accuracy to which this free-drop ensemble of data can define its value. We computed the standard error for each quantity at each station at each 25 m depth interval. The contoured details of these statistics are not revealing in themselves and will not be presented here. Table 4 lists the cross-section mean absolute amplitude of each flux component, together with the standard error. In the following figures of these distributions, the statistically significant contours are those whose values exceed the mean standard error; significant areas of highs, lows, and changes in sign are thus defined.

It is interesting to note that in spite of the well defined distributions of $\overline{u'^2}$, $\overline{v'^2}$, $\overline{\rho'^2}$, the quantities $\overline{u'v'}$, $\overline{u'\rho'}$, $\overline{v'\rho'}$ are statistically less well defined. We also computed the correlation coefficient distributions, $R_{\overline{u'v'}} \equiv \overline{u'v'}/\sqrt{\overline{u'^2}\overline{v'^2}}$, $R_{\overline{u'\rho'}} \equiv \overline{u'\rho'}/\sqrt{\overline{u'^2}\overline{\rho'^2}}$, $R_{\overline{v'\rho'}} \equiv \overline{v'\rho'}/\sqrt{\overline{v'^2}\overline{\rho'^2}}$. Table 4 lists the area mean values of these correlation functions. The distributions of the correlation functions within the area fairly well follow the highs and lows of the numerator. This indicates that the gradients in $\overline{u'v'}$, $\overline{u'\rho'}$ and $\overline{v'\rho'}$ are due to horizontally and vertically changing phase relationships of the fluctuations within the Florida Current, rather than to the variation of the amplitude of the fluctuating signal.

Fig. 7 displays the distributions of the components $\frac{1}{2}\overline{u'^2}$, $\frac{1}{2}\overline{v'^2}$, $\frac{1}{2}\overline{T'^2}$. The values of these quantities recorded by the current meters are superimposed on this figure. The largest values of $\overline{u'^2}$ and $\overline{v'^2}$ occur to the west of the axis of maximum mean northward flow. A second maximum of $\overline{v'^2}$ occurs over the steepest portion of the topographic slope and in the deep channel, similar to a first cross-channel mode. Current meter records indicate a 180° phase change of the northward velocity fluctuations where the energy density is the minimum (Wunsch and Wimbush,

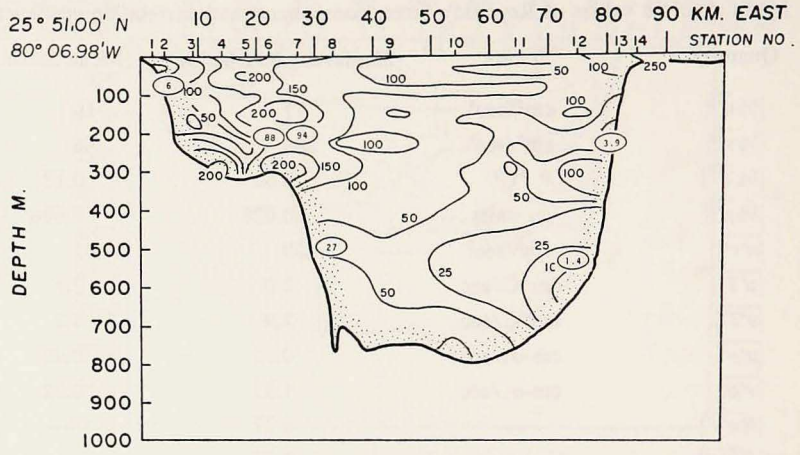

Figure 7a. The distribution of eastward component of perturbation kinetic energy density per unit volume, $\frac{1}{2}\overline{u'^2}$. Area mean of standard error is 16 cm sec^{-2}. The contours are in units of cm^{2}sec^{-2}.

1977). The largest temperature variability is within the main thermocline. When $\overline{\rho'^2}$ is normalized by $\frac{\rho_o}{g}\frac{\partial \overline{\rho}}{\partial z}$, (see Line (3a)) its maximum value also follows the main thermocline between 24.0 and 26.0 σ_t (see Fig. 15a). For all three distributions, there is considerable energy in the easternmost portion of the section which is related to the strong tidal flushing of the Bahama Banks (Brooks, 1977) and to

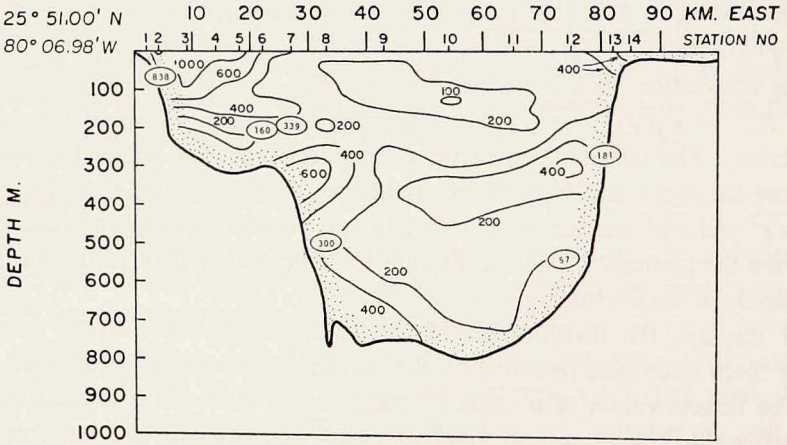

Figure 7b. The distribution of northward component of perturbation kinetic energy density per unit volume, $\frac{1}{2}\overline{v'^2}$. Area mean of standard error is 66 cm^{2}sec^{-2}. The contours are in units of cm^{2}sec^{-2}.

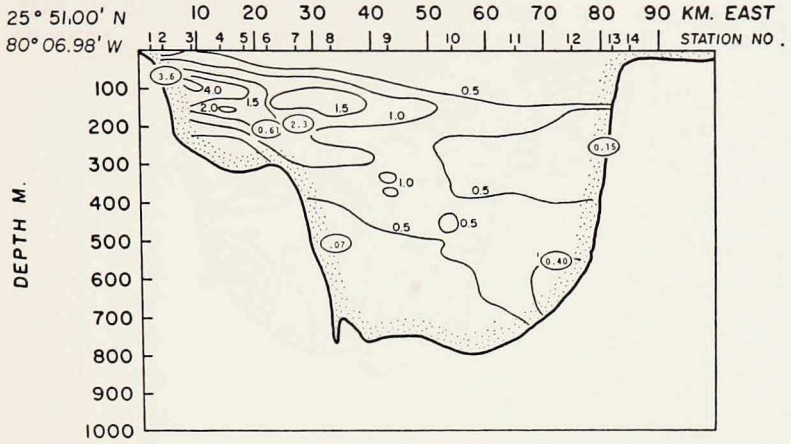

Figure 7c. The distribution of temperature variance, $\frac{1}{2}\overline{T'^2}$. Area mean of standard error is 0.17°C². The contours are in units of °C².

the eddy motions which are presumably due to the three-dimensional changes of the orography of the eastern boundary of the Florida Straits.

The distributions of $\overline{u'v'}$ on the ocean surface were computed at a similar latitude by Webster (1965) and Schmitz and Niiler (1969). Fig. 8 is a comparison of the

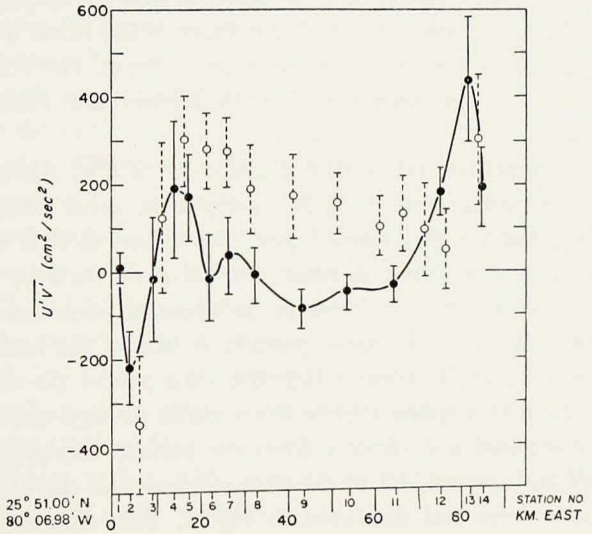

Figure 8. The surface distribution of $\overline{u'v'}$. The solid circles are computed from 1974 data. The open circles are from Schmitz and Niiler (1969). The vertical bars are the standard error of the mean.

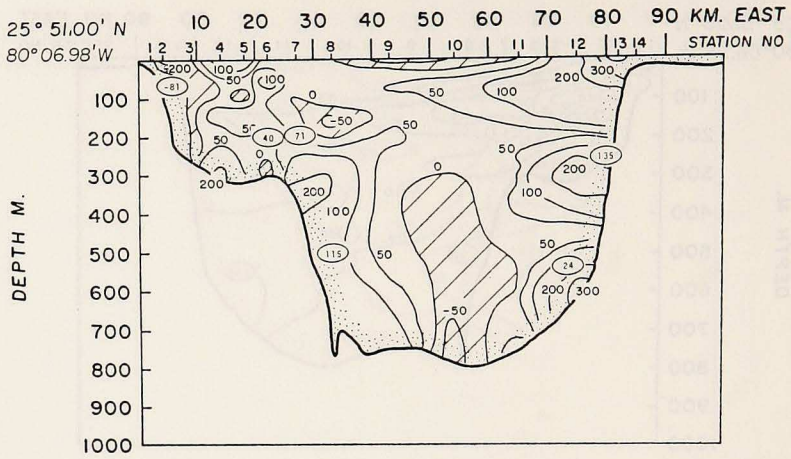

Figure 9. The distribution of $\overline{u'v'}$. The mean standard error is 45 cm^2sec^{-2}. The contours are in units of cm^2sec^{-2}.

surface distribution of this variable from the dropsonde data sets, together with the standard error of the mean. It is interesting to note the differences in the calculation reported by Schmitz and Niiler (1969) and the present calculation, although both sets of surface current observations were obtained by measuring the surface displacement of identical vertically ballasted rods. In the western portion of the Straits, the distributions are quantitatively different. The 1974 data set more nearly resembles the G.E.K. data set reported by Webster, in that a single positive maximum of $\overline{u'v'}$ occurs in the region of strong cyclonic shear of the mean flow, and $\overline{u'v'}$ is a small, negative quantity in the region of anticyclonic shear. The surface distribution of $\overline{u'v'}$ from the historical summer data follows Schmitz and Niiler's (1969) computation.

Fig. 9 displays horizontal and vertical distribution of $\overline{u'v'}$. Although weak negative values appear near the surface, at 50 m depth the cross-straits distribution of $\overline{u'v'}$ closely follows the values obtained from the historical data sets. Clearly, we would not place much confidence in small vertical scale features of a distribution if these occur only at one station; however, independent measurements at Stations 9, 10, and 11 show the aforementioned pattern. A bias of the surface values might result from using a spline fit, even though five data points are used to define the curve at this location. Our spline routine fits a curve through the data in an r.m.s. sense. We also computed $\overline{u'v'}$ directly from the surface current observations and from the first half and second half of the data set; however the distribution did not significantly change from that displayed in Fig. 8. This difference cannot be explained by rotating the axes into the plane of the mean flow. Our conclusion is that the surface conditions (perhaps surface winds) in the summer of 1974 were different than those in 1965-1969 because we do not believe that there are real changes in

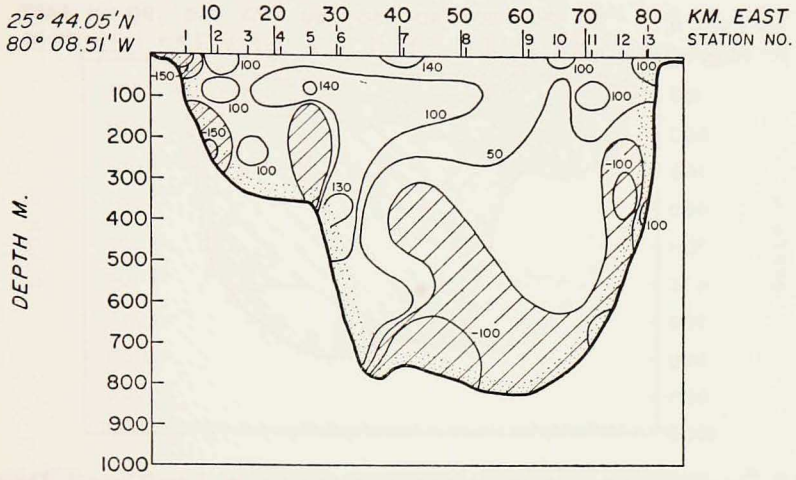

Figure 10. The distribution of $\overline{u'v'}$ from the historical data. The contours are in units of cm^2sec^{-2}.

the energetics of the flow in the center of the Straits within a 12 km distance. However, such a thin layer hardly contributes to the overall, bulk energy or momentum balance of the Florida Current.

Fig. 10 displays the vertical and horizontal distributions of $\overline{u'v'}$ from the historical data. For this calculation, u' and v' are computed from polynomial fits to the average current over the entire depth interval. A comparison of Fig. 10 with Fig. 9 presents some noteworthy features. In both figures, a significant area of negative values is found in the easternmost section of the Straits which changes to a positive maximum within the cyclonic shear-zone of the northward flow. The orientation of the major axis of the variance ellipse, as defined by the angle $\frac{1}{2}\tan^{-1}(2\overline{u'v'}/(\overline{v'^2}-\overline{u'^2}))$ (with respect to the magnetic north), changes from a westward declination to an eastward declination with respect to the mean flow vector. The coastline in the western portion of the Straits is oriented due north. In contrast, near the bottom of Stations 5 and 6, 9-11, and 12-14, the orientation of the variance ellipse tends to follow the major bathymetric features in Fig. 1. This phenomenon of "bottom steering" of low-frequency oscillations when strong bottom gradients are present is observed in other areas of the ocean (for example, on the continental shelf of the eastern Gulf of Mexico, Niiler, 1976; and on the New England continental shelf, Schmitz, 1974). Although not shown in Fig. 1, the plateau between Stations 3 and 6 narrows to the northwest.

Fig. 11 displays the distribution of $\overline{u'T'}$. This distribution shows a pattern from the surface to 100 m which is described by Oort (1964) for the Florida Current off Jacksonville. As in this figure, the general shape of a 50 m thick region of positive

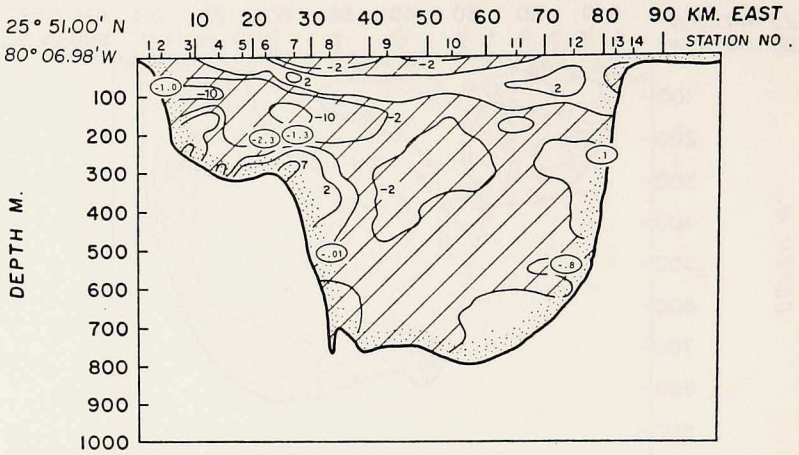

Figure 11. The distribution of $\overline{u'T'}$. The mean standard error is 2.1 cm°C sec^{-1}. The contours are in units of cm°C sec^{-1}.

flux, imbedded in a generally negative distribution, is clearly indicated in Oort's Table 2. The cross-strait turbulent transfer of heat is proportional to $\overline{u'T'}$. In the region of positive values of $\overline{u'T'}$ which follows the contour of the 27°C mean isotherm, the eddy heat transport is offshore. If $\overline{u'T'}$ were the only significant component of eddy heat transport, then the distribution displayed in Fig. 11 would imply that following the mean motion, the eddy transport convergence would tend to strengthen a horizontal temperature gradient at the 250 m depth between Stations 6, 7, and 8 and diminish the horizontal temperature gradient near the surface.

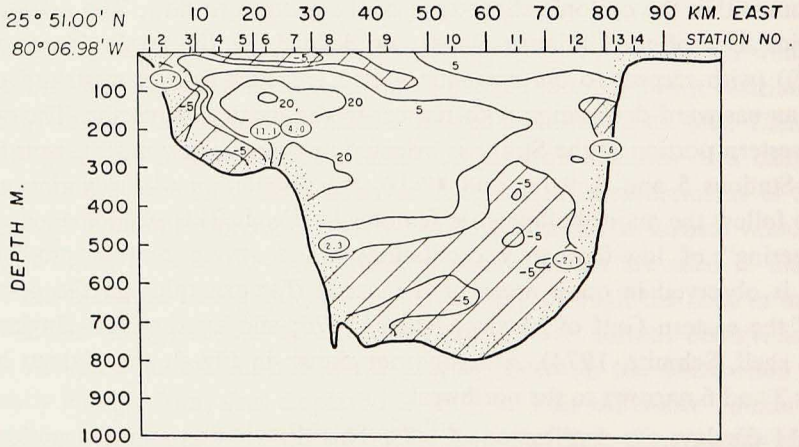

Figure 12. The distribution of $\overline{v'T'}$. The mean standard error is 4.3 cm°C sec^{-1}. The contours are in units of cm°C sec^{-1}.

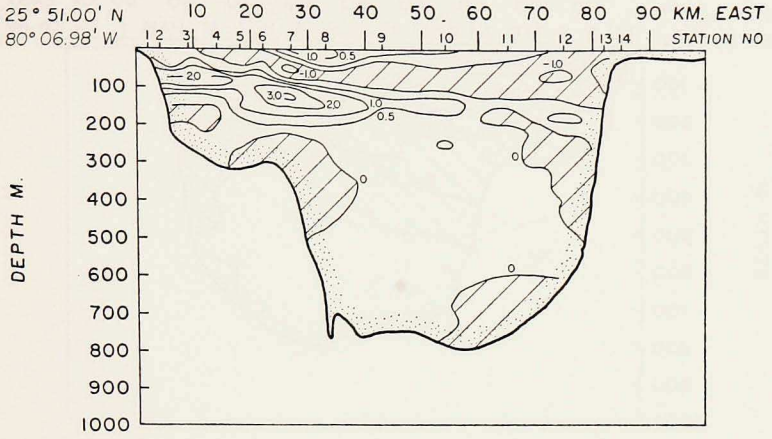

Figure 13. The distribution of $\overline{u'\rho'}$. The mean standard error is 0.40 cm$\sigma_t$sec^{-1}. The contours are in units of cm$\sigma_t$sec^{-1} (ρ' is measured in σ_t units).

The distribution of $\overline{v'T'}$ is displayed in Fig. 12. A northward acceleration of the flow over the greater portion of the main thermocline is associated with a warming trend. Brooks and Niiler (1975) describe an identical phenomenon within the Florida Current south of Key West. The process is of opposite sign near the bottom. The maximum positive value of $\overline{v'T'}$ occurs in the same location as the maximum negative value of $\overline{u'T'}$. In contrast to the distribution of $\overline{v'^2}$ which shows a bimodal structure in the horizontal, $\overline{v'T'}$ displays a bimodal structure in the vertical. Because there is no data base from which to compute $\frac{\partial}{\partial y}(\overline{v'T'})$, the convergence of the northward turbulent flux and its effect on the mean temperature structure cannot be estimated.

Figs. 13 and 14 display the distributions of $\overline{u'\sigma'_t}$ and $\overline{v'\sigma'_t}$ which parallel Figs. 11 and 12 because, as previously discussed, over the greater portion of the experiment, the density is computed from the (T,σ_t) correlation function (Fig. 2).

6. Calculation of the energy exchange

A summary of the calculation of the gross energy distribution within the Florida Straits is presented in Table 1 and in Section 2. In this section, we will discuss in more detail the calculations which lead to these conclusions. The principal conclusion is that, at the Miami latitude, the fluctuations exchange very little net energy with the mean flow; if the net energy exchange rate is of similar amplitude along the entire length of the Florida Current, a doubling or halving of the perturbation energy density could not occur within the time required for the water-mass to travel from the Straits of Yucatan to Cape Hatteras, North Carolina. It is plausible that the fluctuations receive their energy from external sources. Several accompanying

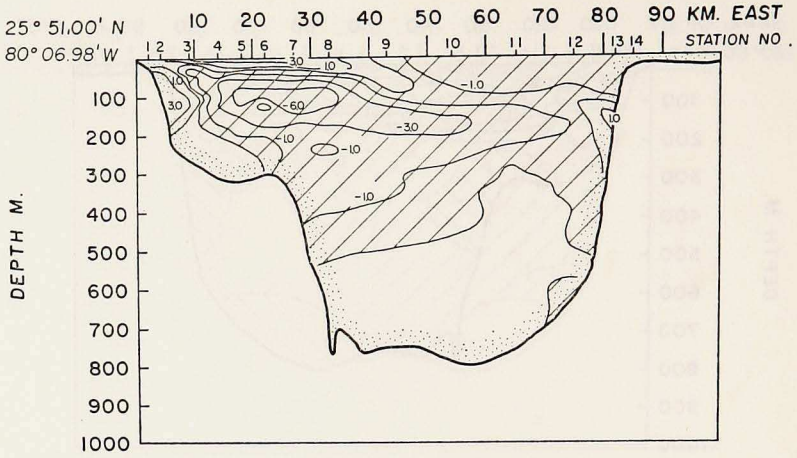

Figure 14. The distribution of $\overline{v'\rho'}$. The mean standard error is 0.72 cm$\sigma_t$sec^{-1}. The contours are in units of cm$\sigma_t$sec^{-1} (ρ' is measured in σ_t units).

papers in this volume of *J.M.R.* (Wunsch and Wimbush, 1977; Düing, Mooers and Lee, 1977), as well as earlier investigations (Webster, 1961b; Niiler, 1969), point to the strong coherence between meteorological events and the variability within the Florida Current. The problem of why the mean flow does not provide energy to the fluctuations is an enigma because theoretical calculations indicate that in an ocean current such as the mean Florida Current, a linear conversion of both available potential energy and kinetic energy to perturbations can occur on a time scale of a few days (for example, see Niiler and Mysak, 1971, and Orlanski and Cox, 1973). Perhaps this linear conversion process is rapidly initiated in the Caribbean, south of the Yucatan channel, while at the Miami latitude finite amplitude perturbations are already in equilibrium with the Florida Current. This would be a condition in which the total energy of the fluctuations no longer grows (the area average of the left-hand side of Equation 3 is "small") while significant fluctuations and local conversion rates are present.

The local distributions of the energy conversion rates do not correspond in detail with the area average picture. It is important to note that the area average of the absolute value, or the mean amplitude, for each conversion term on the right-hand side of Equation 3 is always larger than the area average.

The individual components of the kinetic energy distribution, $\frac{1}{2}\overline{u'^2}$ and $\frac{1}{2}\overline{v'^2}$, are presented in Figs. 7a and 7b. The potential energy distribution, $\frac{1}{2}g\overline{\rho'^2}/\rho_o\left|\frac{\partial\bar{\rho}}{\partial z}\right|$, is displayed in Fig. 15a. The largest value occurs within the main thermocline, under the surface axis of the maximum mean northward flow, while the largest value of $\frac{\overline{\rho'^2}}{2}$ (or $\overline{T'^2}$, Fig. 7c) occurs further to the west in the cyclonic shear zone.

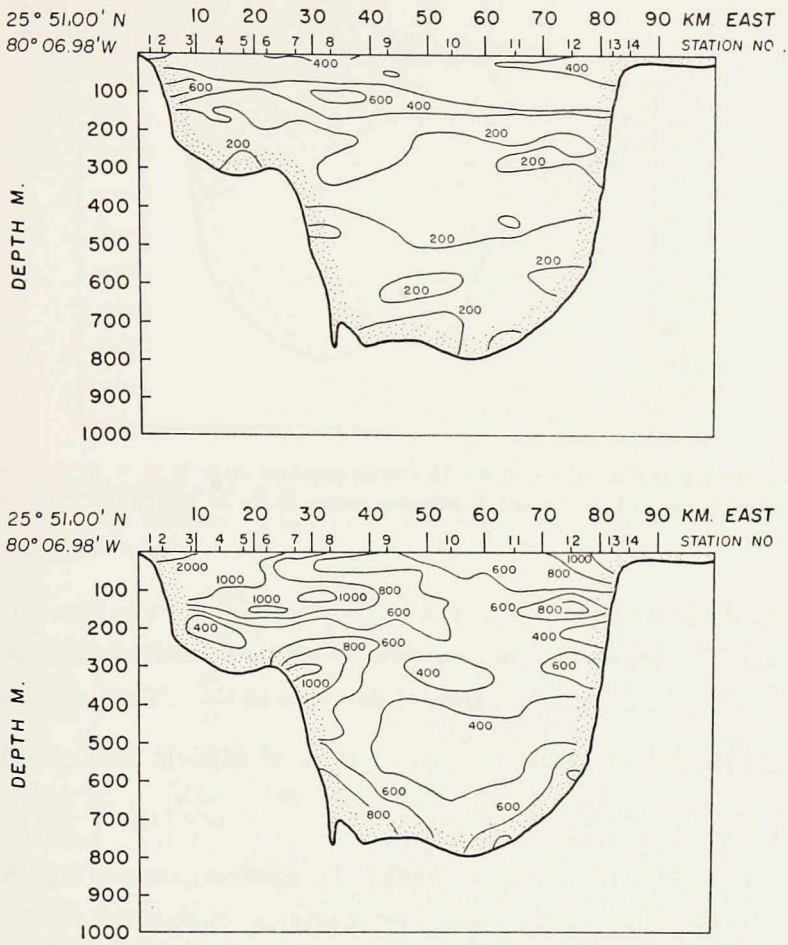

Figure 15a. The perturbation potential energy density distribution per unit volume, $\frac{g}{2}\overline{\rho'^2}/\rho_o \left| \frac{\partial \bar{\rho}}{\partial z} \right|$. The mean standard error is 70 cm^2sec^{-2}. The contours are in units of cm^2sec^{-2}.

Figure 15b. The total perturbation energy density per unit volume, $\frac{1}{2}\overline{u'^2} + \frac{1}{2}\overline{v'^2} + \frac{g}{2}\overline{\rho'^2}/\rho_o \left| \frac{\partial \bar{\rho}}{\partial z} \right|$. The mean standard error is 153 cm^2sec^{-2}. The contours are in units of cm^2sec^{-2}.

The distribution of the total perturbation energy is remarkably uniform through the deep channel (Fig. 15b); the cyclonic shear-zone of the mean northward flow is the most energetic region. From infared images of the sea-surface temperature patterns, we know that this eddy activity intensifies northward along the entire eastern seaboard, and that there is a vigorous exchange of water-mass between the Florida Current and the continental shelf (Lee and Mayer, 1977; Legeichis, 1975; Von Arx, Bumpus, and Richardson, 1955).

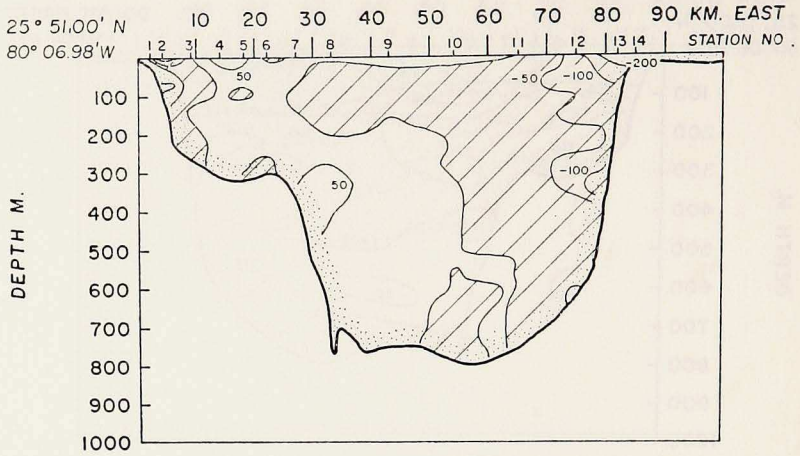

Figure 16. The distribution of $\overline{u'v'}\partial\bar{v}/\partial x$. The mean standard error is 15×10^{-4}cm^{2}sec^{-3}. The contours are in units of 10^{-4}cm^{2}sec^{-3}. Negative values imply an energy flux to the perturbations.

The distributions of $\overline{u'v'}\,\dfrac{\partial\bar{v}}{\partial x}$ and $g\overline{u'\rho'}\,\dfrac{\partial\bar{\rho}}{\partial x}\Big/\rho_o\left|\dfrac{\partial\bar{\rho}}{\partial z}\right|$ are in Figs. 16 and 17, respectively. To compute the errors in these quantities (as well as the terms which follow) we compute the standard error of the mean of $\dfrac{\partial\bar{v}}{\partial x}$, Err $\left(\dfrac{\partial\bar{v}}{\partial x}\right)$, from observations of individual values of $\dfrac{\partial v}{\partial x}$ from pairs of adjacent stations. The total standard error is Err $\left(\overline{u'v'}\dfrac{\partial\bar{v}}{\partial x}\right)$ = (Err $(\overline{u'v'})$) $\dfrac{\partial\bar{v}}{\partial x}$ + $(\overline{u'v'})$ (Err $\left(\dfrac{\partial\bar{v}}{\partial x}\right)$) + (Err $(\overline{u'v'})$) (Err $\left(\dfrac{\partial\bar{v}}{\partial x}\right)$). As mentioned earlier, the significant areas of highs and lows of the distributions are those in which the amplitude exceeds the standard mean error. These are the principal terms of energy exchange from the mean $\bar{v}(x,z)$ linear, quasi-geostrophic, large-scale waves. Note that locally, $\overline{u'v'}\,\dfrac{\partial\bar{v}}{\partial x}$ and $g\overline{u'\rho'}\,\dfrac{\partial\bar{\rho}}{\partial x}\Big/\rho_o\left|\dfrac{\partial\bar{\rho}}{\partial z}\right|$ are the same size. The changes of sign in $\overline{u'v'}\,\dfrac{\partial\bar{v}}{\partial x}$ are principally along vertical lines whereas the changes of sign in $g\overline{u'\rho'}\,\dfrac{\partial\bar{\rho}}{\partial x}\Big/\rho_o\left|\dfrac{\partial\bar{\rho}}{\partial z}\right|$ are along horizontal lines. Because of this orthogonality, there is an impression that the processes which lead to each term operate in a mutually exclusive horizontal and vertical mode. At the moment, we do not know whether each is also governed by different time scale processes. The time series to determine the time scales of these processes certainly exist. If these were the only processes in operation, the sum of the area averages of each term would imply that there is a net flux of energy to the fluctuations from the mean flow and that the perturbation energy within the Current would double in 10 days.

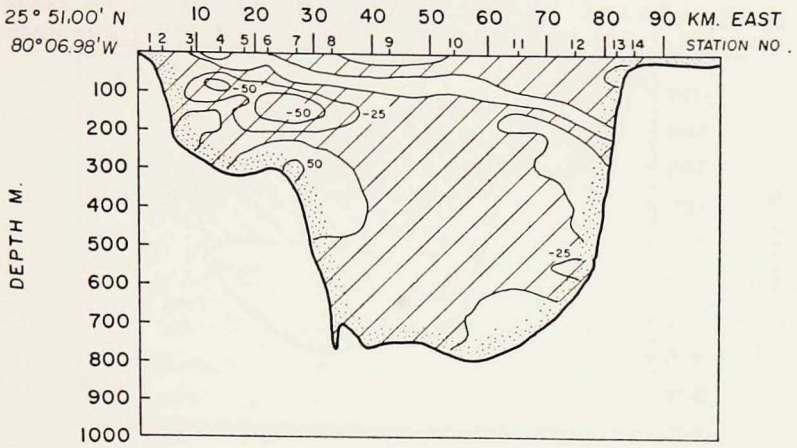

Figure 17. The distribution of $g\overline{u'\rho'}\,\frac{\partial\bar{\rho}}{\partial x}/\rho_o\left|\frac{\partial\bar{\rho}}{\partial z}\right|$. The mean standard error is 13×10^{-4}cm^{2}sec^{-3}. The contours are in units of 10^{-4}cm^{2}sec^{-3}. Negative values imply an energy flux to the perturbations.

The total local conversion rate of mechanical energy is dominated by the term $\overline{v'^2}\,\frac{\partial\bar{v}}{\partial y}$ (note that the area average of this quantity is the smallest of all conversion terms). The total conversion rate of potential energy is dominated by $g\overline{v'\rho'}\,\frac{\partial\bar{\rho}}{\partial y}\Big/\,\rho_o\left|\frac{\partial\bar{\rho}}{\partial z}\right|$. (See net absolute values on Table 1.)

Figs. 18 and 19 display the distribution of the terms in Lines (3c) and (3d), respectively. These net distributions are perhaps endemic to the particular location in the Florida Straits. However, we should stress that because the values of $\overline{v'^2}$ are typically larger than $\overline{u'v'}$ and $\overline{v'\rho'}$ is larger than $\overline{u'\rho'}$, and because the Gulf Stream system (or other western boundary currents) is a three-dimensional flow pattern, the local energy conversions also depend upon the downstream gradients of the mean flow. Externally driven fluctuations in v are especially effective in such a conversion process. We attach no particular significance to Figs. 18 and 19 because we know that the pressure gradients also convert energy locally within the water column, and a local computation must include this effect. Originally, we planned to render a more complete local energy budget by utilizing the bottom pressure records and the hydrographic observations within the Straits to compute the time-dependent pressure field. This did not prove to be practical because of the large tidal signal in the bottom pressure records and our inability to obtain time series of the horizontal currents on the tidal time scale throughout the water column. A second deficiency in the energy budget arises from our inability to compute $\overline{w'p'}$; $\overline{w'p'}$ is the link between potential energy conversion from the mean flow to the

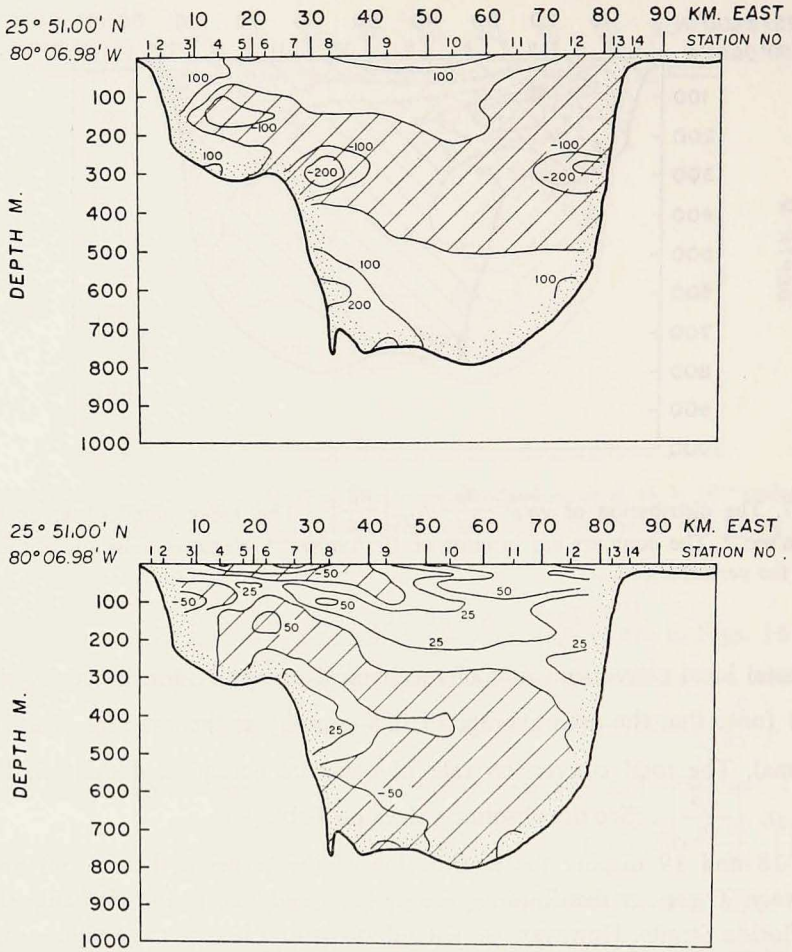

Figure 18. The distribution of the total mechanical energy flux per unit volume to the perturbations $\overline{u'v'}\frac{\partial \bar{v}}{\partial x} + \overline{u'^2}\frac{\partial \bar{u}}{\partial x} + \overline{v'^2}\frac{\partial \bar{v}}{\partial y}$ (Line 3(c)). The mean standard error is 31×10^{-4}cm^{2}sec^{-3}. The contours are in units of 10^{-4}cm^{2}sec^{-3}. Negative values imply a flux to the perturbations.

Figure 19. The distribution of the total potential energy flux per unit volume to the perturbations, $g\overline{u'\rho'}\frac{\partial \bar{\rho}}{\partial x}/\rho_o \left|\frac{\partial \bar{\rho}}{\partial z}\right| + g\overline{v'\rho'}\frac{\partial \bar{\rho}}{\partial y}/\rho_o \left|\frac{\partial \bar{\rho}}{\partial z}\right|$ (Line 3(d)). The mean standard error is 28×10^{-4}cm^{2}sec^{-3}. The contours are in units of 10^{-4}cm^{2}sec^{-3}. Negative values imply a flux to the perturbations.

fluctuations. The total conversion rate, the sum of lines (3c) and (3d), is contoured in Fig. 20.

Finally, it is of some interest to know whether the fluctuations of the scale which we observed could be generated by a vertical, mechanical overturning process, $\overrightarrow{w'v'}$

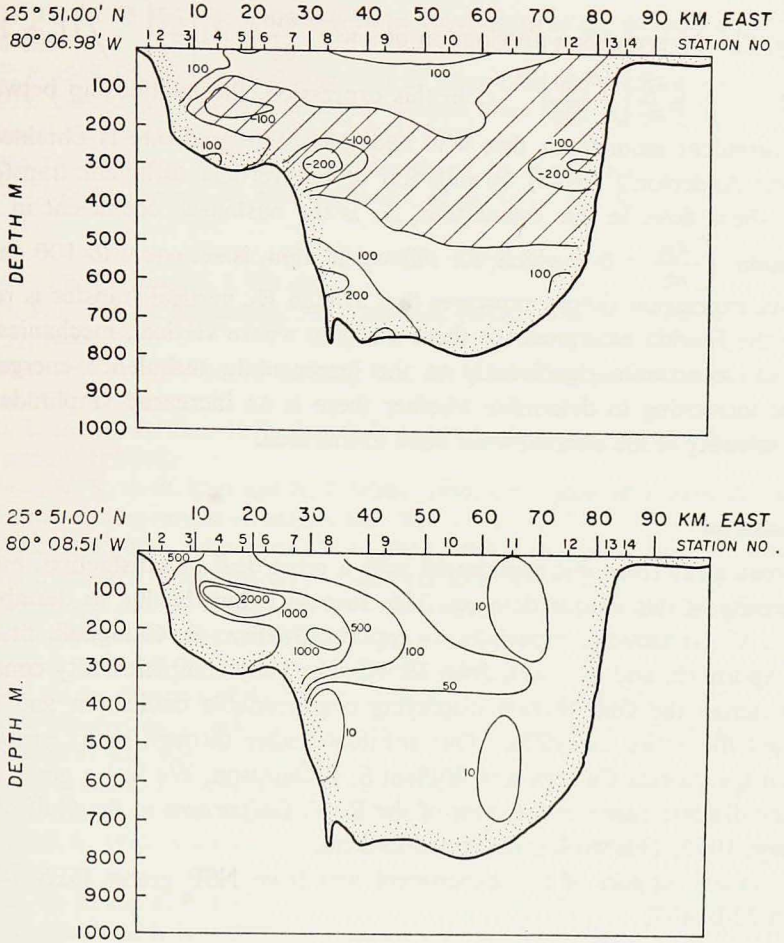

Figure 20. The distribution of the total energy conversion rate, the sum of terms in 3(c) and 3(d). The mean standard error is 59×10^{-4}cm^{2}sec^{-3}. The contours are in units of cm^{2}sec^{-2}.

Figure 21. The distribution of an estimated mechanical energy flux per unit volume to perturbations due to vertical overturning, $-\overline{w'v'}\,\frac{\partial \bar{v}}{\partial z}$ (Line (3e)). The contours are in units of 10^{-5}cm^{2}sec^{-3}. Positive values imply a flux to the perturbations.

$\frac{\partial \vec{v}}{\partial z}$. An estimate of the magnitude of this term can be made from some simple formulations of the vertical transfer in a stratified shear flow. We expect that this transfer occurs in a time scale which is shorter than a pendulum day and longer than the buoyancy period and is not measurable with the free-drop data set, but that its amplitude depends upon the gross 50 m vertical scale shears and stability which were measured. Perhaps more as an item of curiosity than as a representation

of reality, Fig. 21 presents a distribution of $-\overline{w'v'}\,\frac{\partial \bar{v}}{\partial z} = A_o \left|\frac{\partial \bar{v}}{\partial z}\right|^2 \Big/ (1 + 10\,R_i)^{\frac{1}{2}}$, where $R_i = \frac{g}{\rho_o}\left|\frac{\partial \bar{\rho}}{\partial z}\right| \Big/ \left|\frac{\partial \bar{v}}{\partial z}\right|^2$. In this expression, the relationship between the vertical turbulent momentum flux $\overline{w'v'}$ and the mean gradients is obtained from Munk and Anderson's (1948) formulation of the vertical turbulent transfer in a stratified shear flow. In this calculation, A_o is the austausch coefficient in neutral stratification $\left(\frac{\partial \bar{\rho}}{\partial z} = 0\right)$ which, for this calculation, is set equal to 100 cm²/sec². The above expression simply expresses that at high R_i, vertical transfer is reduced. Only on the Florida escarpment is there a region where vertical, mechanical overturning can contribute significantly to the larger scale turbulence energetics. It would be interesting to determine whether there is an increased amplitude of the spectral intensity of the internal wave band in this area.

7. A postscript

We come away from this experiment with a great deal of satisfaction, especially in the quality of this unique data set. This success is largely due to the able crew of the R. V. *Gulfstream*, especially its captain, William B. Campbell, first mate, Jack L. Spornraft, and assistant, John M. Klinck. They completed fifty consecutive ventures across the Gulf Stream displaying commendable dedication and stamina throughout the entire expedition. Our spiritual leader through many years of research on the Florida Current was William S. Richardson. We feel a great sense of loss at the disappearance of the crew of the R. V. *Gulfstream* in the Gulf of Maine in January, 1975. This work is dedicated to them.

The primary support of this experiment was from NSF grants DES 74-02819 and DES 72-01497.

REFERENCES

Brooks, I. H. 1977. High frequency fluctuations in the transport of the Florida Current (in preparation).

Brooks, I. H. and P. P. Niiler. 1975. The Florida Current at Key West: Summer, 1972. J. Mar. Res., *33*, 1.

Düing, W. 1975. Synoptic studies of transients in the Florida Current. J. Mar. Res., *33*, 53–73.

Düing, W., C. N. K. Mooers, and T. N. Lee. 1977. Low frequency variability in the Florida Current and relations to atmospheric forcing from 1972-1974, J. Mar. Res., *35*, this issue.

Iselin, C. 1937. A study of the circulation of the western North Atlantic. Papers in Physical Oceanography and Meteorology, *IV*, 4.

Lee, T. N. and D. A. Mayer. 1977. Low frequency current variability and spinoff eddies on the shelf off southeast Florida. J. Mar. Res., *35*, this issue.

Legeichis, R. 1975. Personal communication.

Lumley, J. L., and H. A. Panofsky. 1964. The structure of Atmospheric Turbulence. Monographs and Texts in Physics and Astronomy. New York, Interscience.

Munk, W. H. and E. R. Anderson. 1948. Notes on a theory of the thermocline. J. Mar. Res., *7*, 276–295.

Niiler, P. P. 1969. On the Ekman divergence in an oceanic jet. J. of Geophys. Res., *4*, 28.

—— 1975. Variability in western boundary currents. Proc. Nat. Academ. Sciences Conf. on Numerical Models of Ocean Circulation, Oct., 1972.

—— 1976. Observations of low-frequency currents on the west Florida continental shelf. Proc. of VII Liege Colloquium on Hydrodynamics, Mem. de la Soc. Roy. des Sci. de Liege, *6*, 331–358.

Niiler, P. P. and L. A. Mysak. 1971. Barotropic waves along the eastern continental shelf. Geophys. Fluid Dynamics, *2*, 273–283.

Niiler, P. P. and W. S. Richardson. 1973. Seasonal variability in the Florida Current. J. Mar. Res., *21*, 144–167.

Oort, A. H. 1964. Computation of the eddy heat and density transports across the Gulf Stream. Tellus, *19*, 1, 55–63.

Orlanski, I. and M. D. Cox. 1973. Baroclinic instability in ocean currents. Geophysical Fluid Dynamics, *4*, 287–332.

Richardson, W. S., A. R. Carr and H. J. White. 1969. Description of a freely dropped instrument for measuring current velocity. J. Mar. Res., *27*, 153–157.

Richardson, W. S., W. J. Schmitz, and P. P. Niiler. 1969. The velocity structure of the Florida Current from the Straits of Florida to Cape Fear. Deep-Sea Res., *16*, 225–234.

Richardson, W. S. and W. J. Schmitz. 1965. A technique for the direct measurement of transport with application to the Straits of Florida, J. Mar. Res., *23*, 172–185.

Schmitz, W. J. 1966. Ph.D. dissertation, University of Miami.

—— 1969. On the dynamics of the Florida Current. J. Mar. Res., *27*, 121–150.

—— 1974. Observations of low-frequency current fluctuation on the continental slope and rise near Side D. J. Mar. Res., *32*, 233–251.

Schmitz, W. J. and P. P. Niiler. 1969. A note on the kinetic energy exchange between fluctuations and mean flow in the surface layer of the Florida Current. Tellus, *21*, 814–819.

Weatherly, G. L. 1972. A study of the bottom boundary layer of the Florida Current. J. P. O., *2*, 54–72.

Weatherly, G. L. and P. P. Niiler. 1974. Bottom homogeneous layers on the Florida Current. Geophys. Res. Let., *1*, 316–319.

Webster, F. 1961a. The effects of meanders on the kinetic energy balance of the Gulf Stream. Tellus, *13*, 392–401.

—— 1961b. A description of Gulf Stream meanders off Onslow Bay. Deep-Sea Res., *8*, 130–143.

—— 1965. Measurements of eddy fluxes of momentum in the surface layer of the Gulf Stream. Tellus, *17*, 239–245.

Von Arx, W. S., D. F. Bumpus, and W. S. Richardson. 1955. On the fine structure of the Gulf Stream front. Deep-Sea Res., *3*, 46–65.

Wunsch, C. and M. Wimbush. 1977. Simultaneous pressure, velocity and temperature measurements in the Florida Straits. J. Mar. Res., *35*, this issue.

Received: *December, 1976.*